Current Photovoltaic Research 4(2) 42-47 (2016)
DOI:http://dx.doi.org/10.21218/CPR.2016.4.2.042
pISSN 2288-3274
eISSN 2508-125X

The Effects of WO_3 Nanoparticles Addition to the TiO_2 Photoelectrode in Dye-Sensitized Solar Cells

Hong Ha Thi Vu · Yoon-Hwae Hwang* · Hyung-Kook Kim*

Department of Nano Energy Engineering and BK21 PLUS Nanoconvergence Technology Division, Pusan National University, Miryang 50463, Republic of Korea

ABSTRACT: Increasing the efficiency of dye-sensitized solar cells (DSSCs) by the fabrication of new photoelectrodes (PEs) is an important challenge. This study examined the photovoltaic parameters of DSSCs composed of a TiO_2 PE with WO_3 nanoparticles (NPs). A number of PEs with the same thickness but different concentrations of WO_3 NPs in the TiO_2PE were prepared. The morphology and structural properties of the prepared PEs were examined by field-emission scanning electron microscopy and X-ray diffraction, respectively. The effects of the WO_3 NPs mixing concentration on the efficiency of DSSCs were investigated under simulated solar light irradiation.

Key words: TiO_2, WO_3, Dye-sensitized solar cells

Nomenclature

V_{OC} : open circuit voltage, V
J_{SC} : short circuit current density, mA/cm^2
FF : fill factor
PCE : power conversion efficiency, %

Subscript

DSSCs : dye-sensitized solar cells
PE : photoelectrode
NP : nanoparticle
FTO : fluorine doped tin oxide
N719 : di-tetrabutylammonium cis-bis(isothiocyanato) bis(2.2'-bipyridyl-4, 4'-dicarboxylato) ruthenium (II)
EIS : electrochemical impedance spectroscopy
XRD : X-ray diffraction
FE-SEM : field emission-scanning electron microscopy
CB : conduction band
VB : valance band

*Corresponding author: yhwang@pusan.ac.kr, hkkim@pusan.ac.kr
Received April 29, 2016; Revised May 13, 2016; Accepted May 25, 2016

1. Introduction

In recent years, solar energy as a green and sustainable energy source has attracted considerable attention in global energy. Among them, dye sensitized solar cells (DSSCs) are relatively inexpensive, efficient, relatively simple to fabricate and clean. Since the first report by Gratzel's group in 1991, DSSCs have been studied to improve their power conversion efficiency (PCE) and are currently undergoing rapid development for practical use[1)]. A basic DSSC consists of a photoelectrode (PE) with a semiconducting thin film with an absorbed ruthenium complex dye deposited on a conducting substrate (fluorine doped tin oxide (FTO)), a counter electrode with FTO glass coated platinum, and a liquid electrolyte containing a redox couple. The light harvesting ability, amount of dye absorption, and the efficiency of charge separation are the three main factors that should be considered when attempting to improve the efficiency of solar cells. Many wide band gap semiconductors have been evaluated as potential electron acceptors for DSSCs, such as TiO_2, ZnO, SnO_2, and Nb_2O_5[1-5)]. Among them, TiO_2 has the highest efficiency because of its high dye absorption and rapid electron transport. Generally, the high efficiency of DSSCs with the photo injected electrons in the TiO_2 are collected at the back contact of the PE in high yield. This requires that the transport time of electrons through the TiO_2 is much faster than their lifetime, which in turn, is determined by the recombination

of electrons with the oxidized dye or with redox couple in the electrolyte. Therefore, it is a factor limiting the efficiency of DSSCs[6]. In addition, a photosensitized dye usually uses a Ru-complex (such as N719, N3), which absorbs photons from sunlight and injects electrons into the conduction band of TiO_2. On the other hand, they only absorb visible light in the wavelength range, 300-800 nm[7,8]. Therefore, most of the solar light is not utilized. If the UV light can be absorbed, the photocurrent of the DSSCs will increase, leading to improved efficiency.

Tungsten oxide (WO_3) is one of the most important n-type semiconductor materials, and a promising candidate for water splitting[9,10], photocatalysis[11,12], DSSCs[13-15], gas sensors[16,17], and electrochromic devices[18,19]. The band gap of WO_3 depends on its crystal structure in the range, 2.6-3.1 eV, which responds to the blue-UV region of the sunlight spectrum[11,13]. Therefore, WO_3 has a smaller band gap than anatase TiO_2 (3.2 eV). In addition, WO_3 has a higher carrier mobility than TiO_2. This study investigated the photovoltaic performance of DSSCs fabricated with the addition of WO_3 NPs. Different concentrations of WO_3 NPs were mixed with TiO_2 NPs to form a PE in DSSC.

2. Experiment

2.1 DSSC fabrication

The TiO_2 (P25) NPs were purchased from Sigma-Aldrich and used as received. The TiO_2 paste was prepared as reported elsewhere[20]. Different amounts of WO_3 NPs powder were dispersed in 5 ml of absolute ethanol under ultrasonication for 15 minutes. Subsequently, 4 ml of a TiO_2 paste was then added and stirred vigorously with a magnetic bar for 3 hours to evaporate the ethanol. The weight ratios of the WO_3 NPs in the TiO_2 NPs paste were 5, 10 and 15 wt.%.

During cell preparation, the FTO glass substrate was cleaned sequentially with deionized water, acetone, and ethanol in an ultrasonic bath. A thin film of TiO_2 mixed with the desired amount of WO_3 NPs was coated uniformly on a FTO glass substrate using the doctor blade method, and dried for 5 minutes at 100°C. The coating procedure was repeated to thicken the mixture layer. The PE was then annealed at 500°C for 1 hour to remove all the organic components. The PE was soaked in a 0.1 M $TiCl_4$ solution at 70°C for 30 minutes, rinsed with water and ethanol, and sintered at 500°C for 1 hour. The prepared PE was immersed overnight in a ruthenium dye solution containing N719 (Solaronix S. A.) in ethanol at room temperature and finally rinsed with pure ethanol, and dried with a continuous flow of nitrogen. The counter electrode was fabricated by the dip-coating of a FTO glass substrate into a chloroplatinic acid H_2PtCl_6 (37.5% Pt basis) solution followed by annealing at 400°C for 30 minutes in air. The cell was assembled by attaching the dye absorbed PE to the counter electrode using a 100 μm hot-melt polypropylene spacer. The liquid electrolyte (Dyesol-TIMO) was injected into the internal space between the sandwiched cell through a hole in the back of the counter electrode, which was sealed using a piece of hot melting film and a cover glass. The other samples were also fabricated using a similar method to compare their efficiency.

2.2 Characterization

The crystal structures of samples were analyzed by X-ray diffraction (XRD, Bruker D8 Discover) using Cu-Kα (λ = 0.15405 nm) radiation in the 2θ range of 10 to 70°. The morphology and composition of these samples were investigated by field-emission scanning electron microscopy (FESEM, Hitachi-S4700). Elemental analysis was determined by energy dispersive X-ray spectroscopy (EDX; Horiba, 6853-H). The current density-voltage curves of the devices were recorded under simulated solar light AM 1.5 G illumination at a light intensity of 100 mW cm^{-2} (Abet Technologies). The active areas of the solar cells were 0.16 cm^2. The electrochemical impedance spectra (EIS) were measured by applying the open circuit voltage under 100 mW cm^{-2} illumination, and the data was recorded over the frequency range, 0.1-100 kHz, using an ac potential pulse with an amplitude of 10 mV. An equivalent circuit model was fitted to the impedance spectra obtained using Z-view software.

3. Results and discussion

3.1 Crystal structures and morphologies

XRD was performed to determine the purity and crystallinity. Fig. 1(a) presents the XRD pattern of the TiO_2 NPs taken in the 2θ scan range, 10-70° . The XRD pattern showed that the TiO_2 NPs have a crystalline structure containing a mixture of anatase (marked as A) and rutile (marked as R) phases. The XRD peaks at 25.3°, 37.8°, 47.9°, 53.8°, 55.0°, 62.4°, and 68.8° were responded to the (101), (004), (200), (105), (211), (204), and (116) planes of anatase TiO_2 phase (JCPDS no. 21-1272), respectively. The peaks at 27.5°, 36.1°, 41.0°, and 56.6° were assigned to the (110), (101), (111) and (220) planes of the rutile phase (JCPDS no. 21-1276), respectively. No additional peak of other phases were detected. Fig. 1(b) shows the XRD pattern of

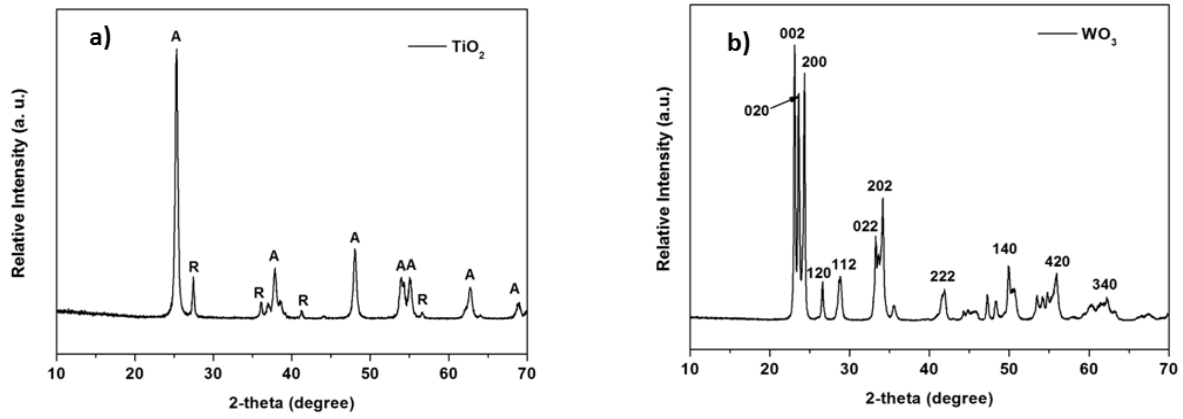

Fig. 1. The XRD patterns of TiO_2 (a) and WO_3 (b)

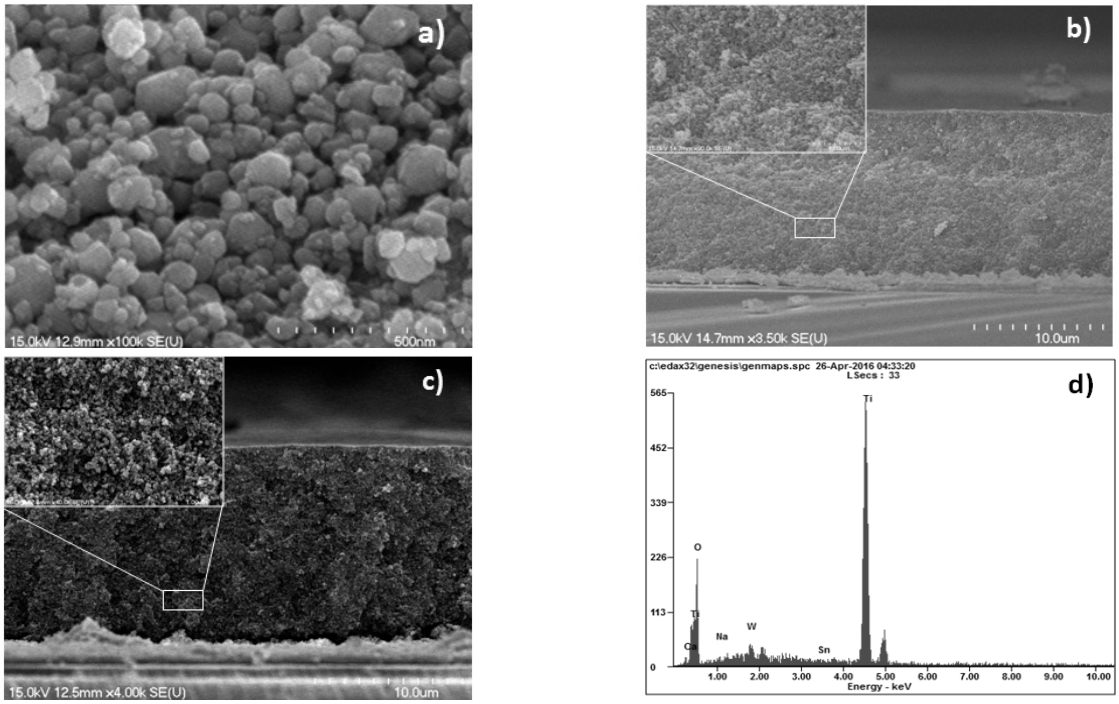

Fig. 2. FE-SEM images of WO_3 nanoparticles (a), low (scale bar 10 μm) and high (scale bar 1 μm) magnification FE-SEM images of the photoelectrode composed of TiO_2 (b) and TiO_2/WO_3 (c). EDX analysis of the TiO_2+ 10%WO_3 PE surface (d)

the WO_3 powder. The results confirmed the formation of pure monoclinic WO_3 crystalline phase (JCPDS no. 43-1035) without any impurity peaks[21]. The XRD peaks are sharp and strong indicating a high crystallinity of samples.

Fig. 2(a) shows FE-SEM images of the WO_3 NPs. The WO_3 particles were separated with a mean particle size ranging from 50 to 200 nm. Fig. 2(b) and (c) present cross-sectional FE-SEM images of the photoelectrode coating on a FTO glass substrate. The thin film of the PEs was uniform and contained compact TiO_2 P25 particles, approximately 14 μm in thickness, whereas the thickness of the TiO_2 + 10% WO_3 particles mixture layer was approximately 13.8 μm. The different concentrations of WO_3 particles PE were prepared using a similar method. The morphology of the TiO_2 mixed with 5% and 15% WO_3 NPs PEs were similar to the mixture TiO_2 + 10% WO_3 particles PE (data not shown). Because small amount of WO_3 particles in the TiO_2 colloid, WO_3 nanoparticles in the mixture PE could not be observed. The EDX analysis of the TiO_2+10%WO_3 PE was performed to present of WO_3 NPs within TiO_2. Fig. 2(d) shows the spectra revealed the present of Ti, O, and W elements on the surface of the TiO_2+10%WO_3 PE. Besides, the Ca, Na, Sn elements are from FTO glass. Therefore, WO_3 particles were confirmed to be present in TiO_2 NPs.

3.2 Photoelectrochemical characterization

Fig. 3 presents the current density- voltage characteristics of the different PEs of DSSCs under simulated 1.5 AM solar illumination. Table 1 lists the measured corresponding parameters with the photocurrent density (J_{SC}), open-circuit voltage (V_{OC}), fill factor (FF), and power conversion efficiency (PCE) of the solar cells. The current density, J_{SC}, of the devices with WO_3 were higher than that of the TiO_2 only devices (Table 1). The maximum current density was 13.36 mA/cm^2 for the DSSC with TiO_2+10%WO_3 PE. The current density increased with increasing WO_3 concentration until the weight ratio was10%, beyond which, J_{SC} decreased. The enhanced J_{SC} originated mainly from the absorption of the blue-UV region of the sunlight spectrum owing to the low band gap of WO_3, which results in more incident solar light being harvested and an enhanced J_{SC}.

The open circuit voltage generated under illumination corresponds to the difference between the Fermi level of the electron in the semiconductor and the redox potential of the electrolyte. The open circuit voltage, V_{OC}, of the DSSC with TiO_2 particles PE was the highest compared to the other DSSCs examined and V_{OC} decreased with increasing concentration of WO_3 NPs in TiO_2. The decreasing V_{OC} was attributed to the conduction band gap edge position of WO_3 being more positive than TiO_2; it was reported to be in the region of 0 V relative to NHE[14]. Although the DSSCs with the WO_3 NPs have a higher current density but a lower V_{OC} and FF than the cell without WO_3, the device containing only TiO_2 displayed the highest photovoltaic parameters: J_{SC}= 12.23 mA/cm^2, V_{OC}= 0.74 V, FF= 68.70% and PCE= 6.22%. The results were negative because the conduction band (CB) of WO_3 is lower than that of TiO_2 but the valence band (VB) of WO_3 is higher than that of TiO_2[22,23]. Therefore, the band structures in the WO_3/TiO_2 couple do not favor the separation of charge carriers[24]. On the other hand, some W sites can act as charge recombination centers according to the following scheme[22]:

$$W^{6+} + e_{(TiO2)\ CB-} \rightarrow W^{5+}$$

$$W^{5+} + e_{(TiO2)\ VB+} \rightarrow W^{6+}$$

Consequently, WO_3 or TiO_2 itself can be a remarkable recombination center for holes and electrons.

Electrochemical impedance spectroscopy (EIS) was performed for a better understanding of the charge transfer inside the DSSCs. Fig. 4 shows the EIS Nyquist plots of the different PEs of DSSCs and the EIS data was fitted to the corresponding equivalent circuit model using Z-view software. In all EIS spectra, there were two well-defined semicircles. The first semicircle at the high frequency region is related to the impedance of the charge transfer process occurring at the interface of the electrolyte and the counter electrode, whereas the other semicircle at the lower frequency region provides information on the impedance at the TiO_2-WO_3/dye/electrolyte

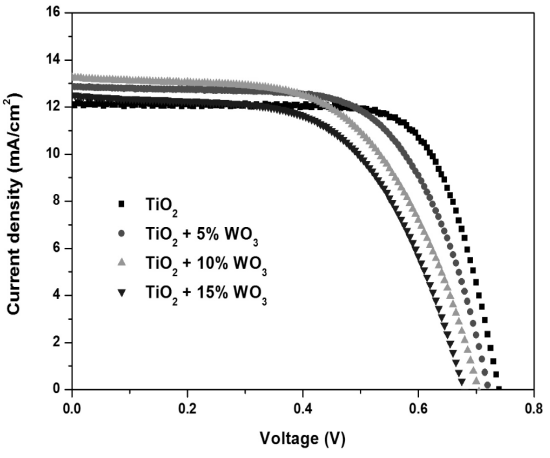

Fig. 3. J-V curves of DSSCs composed with different PEs

Table 1. Performance parameters of DSSCs with different PE types

PE type	J_{SC} (mA/cm^2)	V_{OC} (V)	FF (%)	PCE (%)
TiO_2	12.23	0.74	68.70	6.22
TiO_2 + 5% WO_3	12.92	0.72	63.33	5.89
TiO_2 +10% WO_3	13.36	0.70	57.44	5.38
TiO_2 + 15% WO_3	12.60	0.67	57.44	4.89

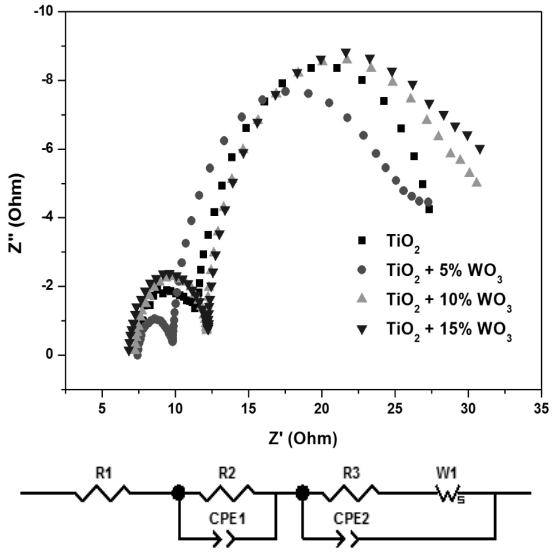

Fig. 4. The EIS Nyquist plots of DSSCs comprised of different PEs and the equivalent circuit model of these DSSCs

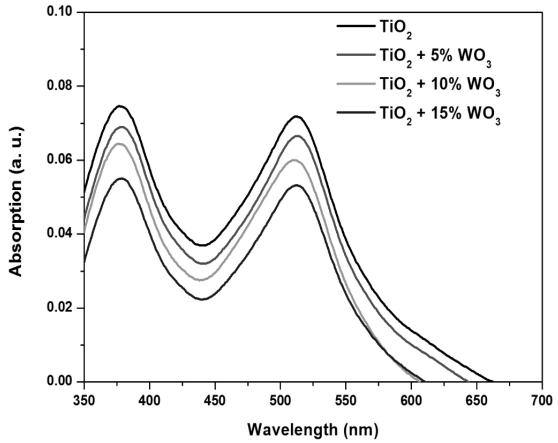

Fig. 5. UV-vis absorption spectra of N719 dye loading in different PEs

interface related to recombination, which is important for determining the efficiency of these DSSCs. The interfacial resistance of the TiO_2/dye/electrolyte was 15.88 Ω for the nanoporous TiO_2 cell. The interfacial resistance of the TiO_2-WO_3/dye/electrolyte was 16.01 Ω, 18.53 Ω, and 18.61 Ω for TiO_2 + 5% WO_3, TiO_2 + 10% WO_3, and TiO_2 + 15% WO_3 PEs in the solar cells, respectively. An increase in the interfacial resistance of the TiO_2-WO_3/dye/electrolyte means an increase in the recombination rate, suggesting a low electron transfer in the cells. As a result, the efficiency of the DSSC with WO_3 particles is reduced.

Generally, a higher level of N719 dye absorption in PEs provides more effective photocurrent generation, which will result in an increase in efficiency. To determine the influence of different concentrations of WO_3 on the performance of the absorbed dye, the loaded dye from the different PEs were estimated by UV-vis absorption spectroscopy.

Fig. 5 represents N719 dye desorption in a 0.1M NaOH solution from the base TiO_2 photoelectrode films and mixed TiO_2 and WO_3 photoelectrode films. The results show that the dye loaded on the bare TiO_2 film was the highest compared to the other PEs and the sensitized dye absorption decreased with increasing amount of WO_3 NPs in the PEs due to the lower surface area of WO_3 compared toTiO_2. Although there was a smaller amount of dye absorbed on the photoanodes containing WO_3 NPs, the photocurrent was enhanced by adding WO_3 to the PEs. This might be because the low band gap of WO_3 responds to the blue-UV region of the solar spectrum. Therefore, the improvement in the photocurrent of DSSC can be attributed to the WO_3 NPs enhancing incident light harvesting.

4. Conclusions

Tungsten oxide nanoparticles were introduced as a photoelectrode in DSSCs. A composite PE with TiO_2 and WO_3 exhibited a higher current density in the cell compared to that using TiO_2 P25 only. On the other hand, the efficiency of the DSSCs with the WO_3 nanoparticles was lower than those without WO_3. These negative results can be explained by the higher recombination rate of holes and electrons and the smaller amount of dye absorbed on the PEs containing WO_3 NPs.

Acknowledgments

This work was supported by a 2-Year Research Grant of Pusan National University.

References

1. O'Regan, B., Gratzel, M., "A low-cost high-efficiency solar cell based on dye sensitized colloidal TiO_2 films," Nature, Vol. 353, pp. 737-740, 1991.
2. Sakai, N., Miyasaka, T., Murakami,T. N., "Efficiency enhancement of ZnO-based Dye-sensitized solar cells by low-temperature $TiCl_4$ treatment and dye optimization," J. Phys. Chem. C, Vol. 117, No. 21, pp. 10949-10956, 2013.
3. Lee, J. H., Park, N. G., Shin, Y. J., "Nano-grain SnO_2 electrodes for high conversion efficiency SnO_2-DSSC," Solar Energy Materials& Solar cells, Vol. 95, pp. 179-183, 2011.
4. Kay, A., Gratzel, M., "dye-sensitized core-shell nanocrystals: Improved Efficiency of Mesoporous Tin Oxide Electrodes Coated with a Thin Layer of an Insulating Oxide," Chem. Mater., Vol. 14, No. 7, pp. 2930-2935, 2002.
5. Le Viet, A., Jose, R., Reddy, M.V., Chowdari, B. V. R., Ramakrisna, S., "Nb_2O_5 Photoelectrodes for Dye-Sensitized Solar Cells: Choice of the Polymorph," J. Phys. Chem. C, Vol. 114, No. 49, pp. 21795-21800, 2010.
6. Paulsson, H., Kloo, L., Hagfeldt, A., Boschloo, G., "Electron transport and recombination in dye-sensitized solar cells with ionic liquid electrolytes," Journal of Electroanalytical Chemistry, Vol. 586, pp. 56-61, 2006.
7. Klein, C., Nazeeruddin, M. K., Liska, P., Censo, D. D., Hirata, N., Palomares, E., Durrant, J. E., Gratzel, M., "Engineering of a novel ruthenium sensitizer and its application in dye-sensitized solar cells for conversion of sunlight into electricity," Inorg. Chem., Vol 44, pp 178-180, 2005.
8. Nazeeruddin, M. K., Kay, A., Rodicio, I., Humphry-Baer, R., Mueller, E., Liska, P., Vlachopoulos, N., Gratzel, M., "Conversion of light to electricity by cis-X2bis(2,2'-bipyridyl-4,4'-dicarboxylate)ruthenium(II) charge-transfer sensitizers (X = Cl-, Br-, I-,

CN-, and SCN-) on nanocrystalline titanium dioxide electrodes," J. Am. Chem. Soc., Vol. 115, pp. 6382-6390, 1993.

9. Liu, X., Wang, F., Wang, Q., Nanostructure-based WO_3 photoanodes for photoelectrochemical watersplitting, Phys. Chem. Chem. Phys., Vol. 14, pp. 7894-7911, 2012.
10. Cristino, V., Caramori, S., Argazzi, R., Meda, L., Marra, G. L., Bignozzi, C. A., "Efficient Photoelectrochemical Water Splitting by Anodically Grown WO_3 Electrodes," Langmuir, Vol. 27, No. 11, pp. 7276-7284, 2011.
11. Wang, F., Valentin, C. D., Pacchioni, G., "Rational band gap engineering of WO_3 photocalalyst for visible water splitting," Chemcatchem, Vol. 4, pp. 476-478, 2012.
12. Szilagyi, I. M., Fórizs,B., Rosseler, O., Szegedi, A., Nemeth, P., Kiraly, P., Tarkanyi, G, Vajna, B., Varga-Josepovits, K., Laszlo, K., Toth, A. L., Baranyai, P., Leskela, M., "WO_3 photocatalysts: Influence of structure and composition," Journal of Catalysis, Vol. 294, pp. 119-127, 2012.
13. Yong, S. M., Nikolay, T., Ahn, B. T., Kim, D. K., "One-dimensional WO_3 nanorods as photoelectrode for dye-sensitized solar cell," J. Alloys Compd., Vol. 547, pp. 113-117, 2013.
14. Zheng, H., Tachibana, Y., Kalantar-zadeh, K., Dye-sensitized solar cells based on WO_3," Langmuir, Vol. 26, No. 24, pp. 19148-19152, 2010.
15. Shaikh, S. F., Kalanur, S. S., Mane, R. S., Joo, O. S., "Monoclinic WO_3 nanorods–rutile TiO_2 nanoparticles core–shell interface for efficient DSSCs," Dalton Trans., Vol. 42, pp. 10085-10088, 2013.
16. Siciliano, T., Tepore, A., Micocci, G., Serra, A., Manno, D., Filippo, E., "WO_3 gas sensors prepared by thermal oxidization of tungsten," Sensors and Actuators B: Chemical, Vol. 133, pp. 321-326, 2008.
17. Zeng, J., Hu, M., Wang, W., Chen, H., Qin, Y., "NO_2-sensing properties of porous WO_3 gas sensor based on anodized sputtered tungsten thin film," Sensors and Actuators B: Chemical, Vol. 161, pp. 447-452, 2012.
18. Papaefthimiou, S., Leftheriotis, G., Yianolis, Y., "Advanced electrochromic devices based on WO_3 thin films," Electrochimia Acta, Vol. 46, pp. 2145-2150, 2001.
19. Liang, L., Zhang, J., Zhou, Y., Xie, J., Zhang, X., Guan, M., Pan, B., Xie, Y., "High-performance flexible electrochromic device based on facile semiconductor-to-metal transition realized by $WO_3 \cdot 2H_2O$ ultrathin nanosheets," Scientific reports, Vol. 3, Acticle number 1936, pp. 1-8, 2013.
20. Vu, T. H. H., Atabaev, T. S., Ahn, J. Y., Nguyen, N. D., Kim, H. K., Hwang, Y. H., "Dye-sensitized solar cells composed of photoactive composite photoelectrodes with enhanced solar energy conversion efficiency," J. Mater. Chem. A, Vol. 3, pp. 11130-11136, 2015.
21. Yang, B., Zhang, Y., Drabarek, E., Barnes, P. R. F., and Luca, V., "Enhanced photoelectrochemical activity of sol-gel tungsten trioxide films through textural control," Chemistry of Materials, Vol. 19, No. 23, pp. 5664–5672, 2007.
22. Zhang, H., Chen, G., Bahnemann, D. W., "Photoelectrocatalytic materials for environmental application," J. Mater. Chem., Vol. 19, pp. 5089-5121, 2009
23. Shaban, A. Y., Khan, S. U. M., "Photoresponse of Visible Light Active CM-n-TiO_2, HM-n-TiO_2, CM-n-Fe_2O_3, and CM-p-WO_3 towards Water Splitting Reaction," Hindawi publishing corporation, Internatinal Journal of Photoenergy, Vol. 2012, article ID 749135, pp. 1-20, 2012.
24. Higashimoto, S., Sakiyama, M., Azuma, M., "Photoelectrochemical properties of hybrid WO_3/TiO_2 electrode. Effect of structure of WO_3 on charge separation behavior," Thin Solid Film, Vol. 503, pp. 201-206, 2006.